CALIBRATION OF EDEM PARAMETERS AND CONSTRUCTION OF A COUPLED DISCRETE ELEMENT MODEL FOR THE SOIL-RESIDUAL FILM MIXTURE IN XINJIANG COTTON FIELDS

/

新疆棉田耕层土壤-残膜混合物 EDEM 参数标定和耦合离散元模型构建

Qizhi YANG*[1)], Zhengliang LI[1)], Qingyu WU[1)], Lei LIU[1)], Ruoyu ZHANG[1)], Xia ZHONG[1)], Guangyi QU[1)], Aiping SHI[2)], Min ADDY[3)]

[1)] School of Agricultural Engineering, Jiangsu University, Zhenjiang 212013, Jiangsu, China;
[2)] School of Vehicle and Traffic Engineering, Jiangsu University, Zhenjiang 212013, Jiangsu, China;
[3)] Bioproducts and Biosystems Engineering Department, University of Minnesota, St. Paul, MN 55108, USA
Corresponding author: Qizhi Yang: Tel: +86 13815172929.; E-mail: qzyrobot@126.com

DOI: https://doi.org/10.35633/inmateh-78-102

***Keywords**: soil-residual film mixture; EDEM model; parameter calibration; plough layer residual film*

ABSTRACT

The recovery of residual film in the plough layer is one of the key bottlenecks that the cotton industry in Xinjiang urgently needs to overcome. The absence of an accurate soil-residual film coupled EDEM model restricts the analysis of the working mechanism and structural optimization of the soil-film separation device in full-feed residual film recovery machines. This study focuses a 20-year continuous cotton field in Korla, Xinjiang, and constructs a soil-residual film coupled EDEM model. The parameters for soil models at various tillage depths were calibrated by employing a steepest ascent approach followed by a Box-Behnken experimental design, with the angle of repose serving as the response metric. The discrepancy between the simulated and experimentally measured angles of repose was less than 0.22%. The EDEM model parameters for residual film in the plough layer were calibrated based on tensile tests using tensile force and elongation as metrics. The calibration achieved errors of 0.16% in tensile force and 0.934% in elongation compared to experimental measurements. Incorporating the distribution patterns of residual film, a coupled EDEM model of the soil-residual film mixture was developed. This model aims to provide a simulation reference for designing the soil lifting and film-soil separation mechanisms of a full-feed plough layer residual film recovery machine.

摘要

耕层残膜回收是新疆棉花产业亟待突破的关键瓶颈之一。而土壤-残膜耦合 EDEM 模型的缺乏，制约了全喂入式残膜回收机膜土分离装置的工作机理分析与结构优化。本研究以新疆库尔勒 20 年连作棉田为对象，构建土壤-残膜耦合 EDEM 模型。采用最陡爬坡法结合 Box-Behnken 实验设计，以休止角为响应指标，对耕层不同深度土壤模型参数进行标定，所得模拟休止角与实测值误差小于 0.22%。基于拉伸试验以拉伸力与伸长率为指标完成耕层残膜 EDEM 模型参数标定，拉伸力与伸长率标定误差分别为 0.16%和 0.934%。结合残膜分布规律构建土壤-残膜混合物耦合 EDEM 模型，该模型旨在为全喂入式耕层残膜回收机的起土装置与膜土分离装置设计提供仿真参考。

INTRODUCTION

Xinjiang is China's major cotton-producing region. In 2024, the cotton planting area in Xinjiang was 2,447.9 thousand hectares, with a total output of 5.686 million tons. One of the key agricultural practices in cotton cultivation is mulch-covered planting, which helps to retain heat and moisture, suppress pests, diseases, and weeds, and significantly increase cotton yields (*Li et al., 2017; Huang et al., 2018*). The cotton fields in Xinjiang predominantly utilize ultra-thin mulch film with a thickness of 0.008 mm, which is relatively low-cost (*Hu et al., 2019*). However, this mulch film exhibits low strength and poor weather resistance, leading to fragmentation after use and making thorough cleanup with surface recovery machinery difficult. Additionally, the high cost of recovery leads to a significant accumulation of residual film in the soil each year (*Yang et al., 2023*). Excessive residual film in the plough layer has severely impaired cotton root growth, resulting in reduced cotton quality and yield, and causing severe residual film pollution problems (*Wang et al., 2025*).

Residual film recovery technology and equipment are the primary means of recovering residual film from the plough layer and addressing pollution issues at present (*Liang et al., 2019*). To study the operational structure and force processes of residual film recovery machines using discrete element simulation methods, it is necessary to establish an accurate simulation model of cotton field soil. To this end, scholars have conducted a certain amount of research on parameter calibration for soil and residual film. Fang et al., employed a DEM-MBD coupled method to establish a simulation model of the tooth-soil-residual film system, optimizing the design of the film-lifting device of the residual film recovery machine (*Fang et al., 2024; Fang et al., 2025*). Jin et al., established a virtual soil trench model of cotton field residual film-soil-straw particles, investigating the soil accumulation effect and conveying devices in terms of soil excavation and conveying efficiency, as well as the characteristics of particle velocity changes (*Jin et al., 2023*). Shen et al selected the Hertz-Mindlin with Bonding contact model to calibrate the parameters of the discrete element model for residual film in the plough layer. By comparing the physical and simulated plough layer residual film states and tensile curves, they validated the plough layer residual film model (*Shen et al., 2024*). Despite progress in soil and residual film modelling, simulation studies specifically addressing the clayey soils of southern Xinjiang cotton fields and the full-feed type plough layer residual film recovery machines remain scarce (*Huang et al., 2024*).

This study investigated the distribution of residual film in the plough layer of Xinjiang's cohesive cotton soils and established a discrete element model integrating residual film and soil. The findings are essential for optimizing the design and dynamics of key residual film recovery machine components, particularly the soil-engagement and film-soil separation mechanisms. In this study, the Hertz-Mindlin with JKR and Hertz-Mindlin with Bonding models were selected as simulation contact models for soil and residual film respectively. Simulation parameters for different plough layer soils were calibrated using the steepest ascent test and Box-Behnken test. Simulation contact parameters for residual film were calibrated using tensile tests, the deformation characteristics of residual film during stretching and tearing are fully considered. Combining the distribution patterns of residual film, a coupled EDEM model of soil-residual film was established. This coupled model can directly support the dynamic simulation and structural optimization of the burial and film-soil separation mechanisms of the plough layer residual film recovery machine, thereby achieving practical effects that are difficult to attain through single-component calibration studies.

MATERIALS AND METHODS

Experimental Material Collection and Preparation

The study area was the Korla region of Xinjiang, with sampling locations in Yuli County, Korla. The sampling area was a cotton-growing region with an average continuous cropping period of 20 years. Sampling was conducted in April 2024 using a five-point sampling method in residual film recovery experimental cotton fields using mulch cultivation. The sampling depth was 200 mm. The sample plot size was 300 mm × 300 mm × 200 mm, and samples were collected in layers at depths of 0–50 mm, 50–100 mm, 100–150 mm, and 150–200 mm. The collected samples were placed in self-sealing bags and numbered from A-1 to E-5, with a total of 25 samples collected.

The residual film was isolated from each soil layer by sieving. Following separation, the film fragments were rinsed with clean water and subsequently dried. The area of each fragment was measured with graph paper. Based on area size, the fragments were categorized into three classes: <4 cm², 4–25 cm², and >25 cm², and the number of pieces in each class was counted. The number of residual film pieces of different areas and their average values for each soil layer are shown in Figure 1.

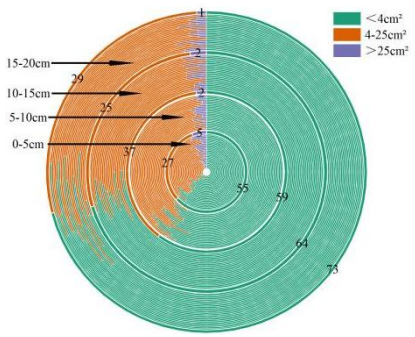

Fig. 1 - Comparison of the number of residual films with different areas and the average number of films in each layer

The total number of residual film pieces showed no significant difference across soil layers, with an approximate ratio of 1:1:1:1. However, residual film pieces smaller than 4 cm² account for the highest proportion in each soil layer, while those larger than 25 cm² account for the lowest proportion in each soil layer.

Parameter Calibration Methods

Determination of Soil Angle of Repose

The angle of repose refers to the angle formed between a material piled on the ground in its natural state and the ground (*Liu et al., 2016; Al-Hashemi et al., 2018*). The angle of repose is closely related to the characteristics of the material, such as density and moisture content. In this study, a homemade angle of repose funnel was used to measure the angle of repose of soils from different depth of plough layer, as shown in Figure 2a. First, 1000 g of plough layer soil was weighed and poured into the funnel from the top, allowing the soil to slide down the inner wall of the funnel. Once the soil had stabilized, an electronic protractor was used to measure the angle of inclination, as shown in Figure 2b. The angle of repose was measured three times for each soil layer, and the average values were calculated. The average angles of repose for the 0–5 cm, 5–10 cm, 10–15 cm, and 15–20 cm soil layers were 44.42°, 45.84°, 47.90°, and 49.72°, respectively.

（a）Funnel （b）Angle of repose

Fig. 2 - Stacking angle measurement test

Residual Film Tensile Test

This study combines tensile physical experiments and EDEM simulation tests to calibrate the discrete element model parameters of residual film in the cotton field plough layer. A texture analyser was used to conduct tensile tests on the residual film. Larger pieces of surface residual film and plough layer residual film were selected and cut into rectangular samples with a width of 20 mm and a length of 60 mm using scissors. The residual film was then fixed in the clamps at the upper and lower ends of the texture analyser, ensuring it remained in a relaxed state. During installation, the residual film was aligned with the testing axis of the texture analyser. The testing speed was set to 5 mm/s, and the analyser was raised at a constant speed until the residual film fractured. The testing process is illustrated in Figure 3.

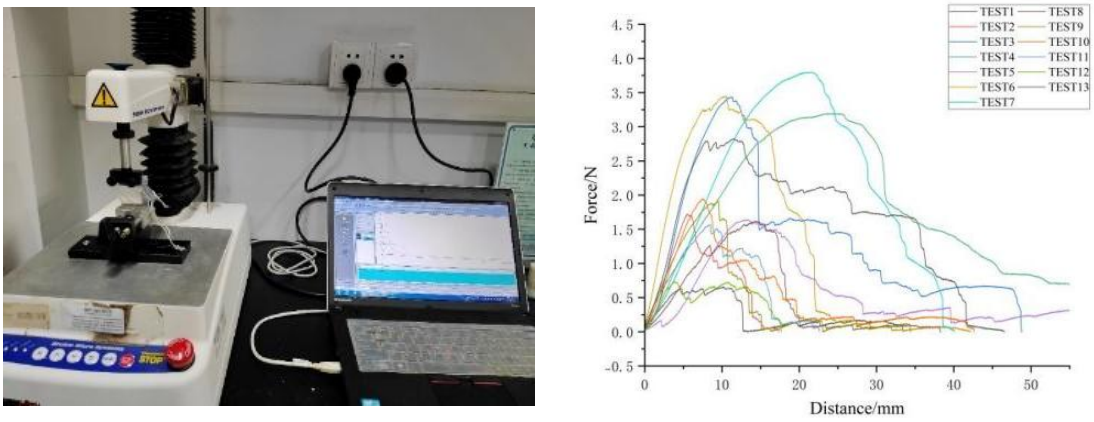

（a）Residual film tensile test （b）Distance and force of residual film

Fig. 3 -Tensile test of residual film in plough layer

SELECTION OF CONTACT MODELS

Selection of Soil Contact Models

The soil types in Xinjiang are primarily sandy soil and sandy loam. However, due to the use of drip irrigation under plastic mulch cultivation technology in cotton fields, moisture is retained in the soil, resulting in high soil moisture content. Consequently, the soil exhibits strong cohesive properties. In this study, the Hertz-Mindlin with JKR model was selected as the contact model for soil particles (*Chen et al., 2023; Zhang et al., 2024*).

The Hertz-Mindlin with JKR (Johnson-Kendall-Roberts) model is a cohesive contact model that accounts for the influence of Van der Waals forces within the contact zone, enabling the modelling of strongly adhesive systems(*Yu et al., 2022; Chen et al., 2025)*. The contact theory formulation of the JKR model is similar to that of the Hertz-Mindlin (no slip) model, both including standard normal and tangential nonlinear adhesion forces and damping effects. However, the JKR model simulates cohesion and adhesion between discrete particles by defining an attractive component.

Selection of Contact Models for Residual Film EDEM Simulation

Tensile tests on the residual film revealed that it exhibits a certain degree of ductility. Therefore, the Hertz-Mindlin with Bonding model was adopted as the contact model for the residual film. In the Bonding contact model, particle models are connected via bonds. These bonds deform under external forces such as tension, compression, or torsion, and fracture when deformation reaches a certain threshold. Considering the limitations of computational capabilities, a particle scaling technique was employed, where larger simulated particles were used to represent the actual smaller conveyed particles (*Queteschiner D., 2018; Feng Y., 2014; Thakur S., 2016*). The relationship between simulated physical quantities and actual particle physical quantities was established through physical scaling factors. By adjusting DEM model parameters, the large-scale discrete element simulation results were made to exhibit the same dynamic and static characteristics as the real small-sized particles (*Li Y., 2019; Ren J., 2017*). In the modelling of scaled particles, Feng proposed three similarity principles: geometric similarity, mechanical similarity, and dynamic similarity. These principles are necessary conditions for a scaled model to accurately replicate the mechanical behaviour of the physical model. All conditions satisfying these similarity principles and ensuring precise equivalence between the physical and scaled models can be summarized as:

$$\frac{R_m}{R_p}=\frac{D_m}{D_p}=\frac{\mu_m}{\mu_p}=\frac{L_m}{L_p}=h \quad (1)$$

$$\frac{F_m(\mu_m,R_m)}{F_p(\mu_p,R_p)}=\frac{A_m}{A_p}=\frac{Q_m(t)}{Q_p(t)}=h^2 \quad (2)$$

where the ratio h is the scaling factor; R and D represent the radius of any particle in the model and the characteristic length of the model domain, respectively. The subscripts m and p denote the scaled model and the physical model. μ represents the overlap/separation/sliding distance between two contacting/adjacent particles, L denotes the representative length of a particle, and A is the surface area. F is the normal or tangential contact force, and Q refers to any external force acting on the particle.

In the Hertz-Mindlin with Bonding contact model, after bond formation, the initial normal and tangential forces, as well as normal and tangential moments between particles, are zero and change with the time step.

The corresponding formulas are as follows:

$$\delta F_n=-V_n S_n A\delta_t \quad (3)$$

$$\delta F_t=-V_t S_t A\delta_t \quad (4)$$

$$\delta M_n=-\omega_n S_t J\delta_t \quad (5)$$

$$\delta M_t=-\omega_t S_n \frac{J}{2}\delta_t \quad (6)$$

where: δF_n and δF_t are the increments in normal and tangential force, respectively, [N]; V_n and V_t are the particle normal and tangential velocities, respectively, [m/s]; S_n and S_t represent the normal stiffness and shear stiffness, respectively, [N/m]; A is the contact area, [m²]; δ_t is the time step, [s]; δM_n and δM_t denote the increments in normal and tangential moment, respectively, [N·m]; J is the polar moment of inertia, [m⁴]; ω_n and ω_t are the particle normal and tangential angular velocities, respectively, [rad/s].

$$A=\pi R_B^{\,2} \quad (7)$$

$$J=\frac{1}{2}\pi R_B^{\,4} \quad (8)$$

where: R_B represents the equivalent contact radius of the bond, [m]. The stress conditions for bond fracture are:

$$\sigma_{max} < \frac{-F_n}{A} + \frac{2M_t}{J} R_B \quad (9)$$

$$\tau_{max} < \frac{-F_t}{A} + \frac{M_n}{J} R_B \quad (10)$$

where: σ_{max} and τ_{max} represent the normal and shear stress, respectively, [Pa].

In this study, length, time, and density were selected as the fundamental quantities, with their scaling ratios being: λL=h，λT=h，λρ=1. In the Bonding model, the scaling ratios for stiffness and stress are h and 1, respectively. By calibrating DEM model parameters such as the equivalent bond contact radius, the simulation results of the residual film discrete element model exhibited the same dynamic and static characteristics as the real residual film. The residual film particle model with dimensions of 60 mm × 20 mm × 0.8 mm was generated by setting the particle radius to 0.2 mm and the contact radius to 0.25 mm.

During tensile simulation tests in EDEM software, based on the operational characteristics of the texturometre in actual tensile tests, the lower jaw is set to remain stationary while the upper jaw rises at a constant speed. As the upper jaw ascends, the residual film model gradually elongates. Upon reaching the tensile limit, a notch forms along the side of the residual film model, subsequently propagating along the notch until complete fracture occurs. The evolution of Bond bonds during stretching is illustrated in Figure 8. Before stretching begins, no Bond connections are under tension, appearing blue (Figure 4a). Upon initiating the simulated test, some Bond connections turn green as they undergo stretching (Figure 4b). At the tensile limit, a small portion of Bond connections turn red (Figure 4c), followed by fracture. The fractured bonds revert to blue (Figure 4d), and upon complete fracture (Figure 4e), all Bond bonds return to blue (Figure 4f). The residual film model retracts to a certain extent before stabilizing.

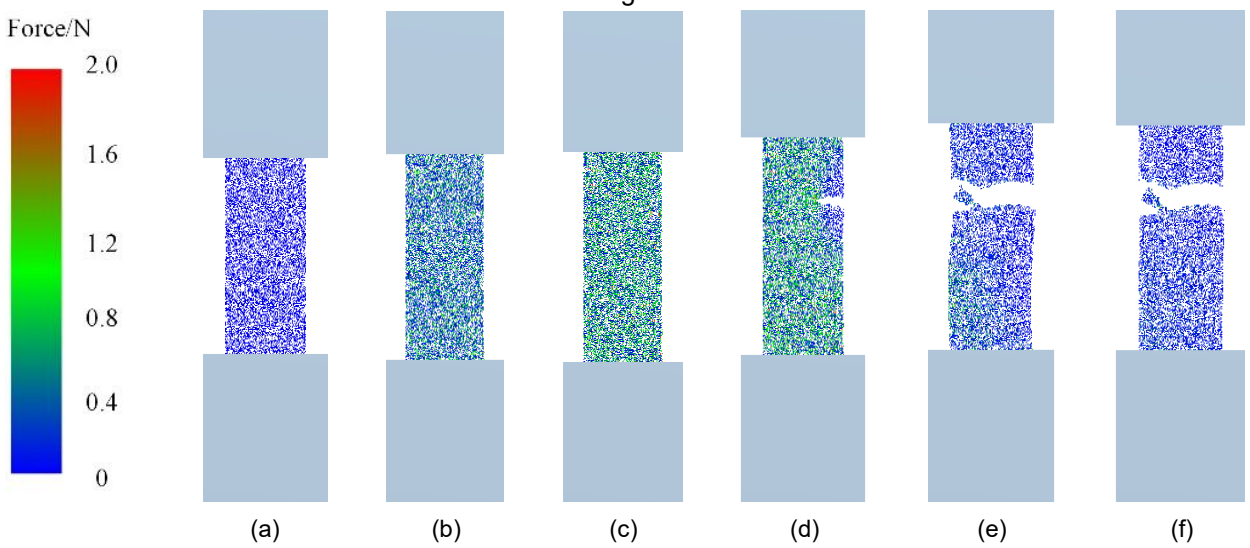

Fig. 4 - Tensile process of residual film model simulation test

The Coupled EDEM Model Construction

First, multiple particle models were created within the Bulk Material module: 0-50 mm soil particles, 50-100 mm soil particles, 100-150 mm soil particles, 150-200 mm soil particles and residual film particles. Simulation parameters are shown in Table 1.

Table 1

Simulation characteristic parameters table

Parameter	Value
Residual film shear modulus	8.3×10^8Pa
Residual film density	0.91g/cm^3
Residual film Poisson's ratio	0.42
Residual film - residual film static friction coefficient	0.65
Residual film - residual film kinetic friction coefficient	0.43
Residual film - residual film collision recovery coefficient	0.86
Soil - residual film collision recovery coefficient	0.31
Soil - residual film static friction coefficient	0.68
Soil - residual film kinetic friction coefficient	0.28

When establishing Meta-Particle models for residual film in plough layers of different sizes using the coordinate method, residual film areas were categorized as <4 cm², 4–25 cm², and >25 cm². Corresponding Meta-Particle models were created with dimensions of 10×20 mm, 20×60 mm, and 40×90 mm, respectively. Given that particle size significantly impacts simulation speed in EDEM, a block-based modelling approach was adopted for mixture models to accommodate computational constraints. Separate models will be created for: 0-50 mm residual film-soil mixture, 50-100 mm residual film-soil mixture, 100-150 mm residual film-soil mixture, 150-200 mm residual film-soil mixture model. Combining the distribution quantities of residual film across different areas within the plough layer, residual film models of varying sizes will be generated. These residual film models and soil models will be randomly generated simultaneously and allowed to fall freely. The generated soil-residual film mixture models at different depths will be saved separately and then imported into the coupled EDEM model. Four particle factories were then created for the residual film-soil mixtures at depths of 0-50 mm, 50-100 mm, 100-150 mm, and 150-200 mm. The complete coupled EDEM model of residual film and soil in the plough layer is shown in Figure 5.

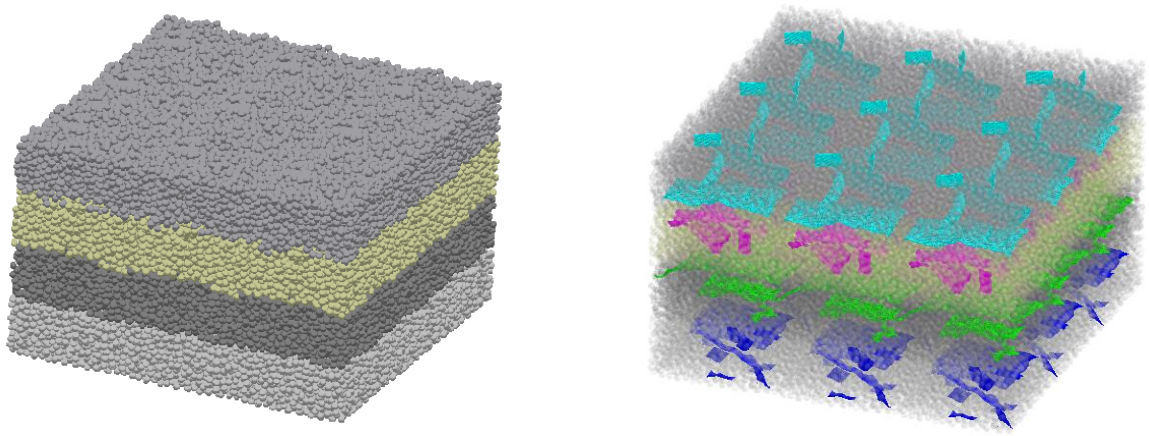

（a）The coupled EDEM particle model (b) Distribution of residual film in soil

Fig. 5 - Construction of the coupled EDEM particle model

RESULTS AND DISCUSSION

Calibration of the Soil EDEM Model

A layered modelling approach was adopted to construct the soil-residue film EDEM model. EDEM parameter calibration experiments were conducted for soil layers at depths of 0–50 mm, 50–100 mm, 100–150 mm and 150–200 mm. Based on literature (*Hu et al., 2021; He et al.,2022; Li et al., 2024*), the inter-soil JKR surface energy X1, collision recovery coefficient X2, and kinetic friction coefficient X3 were selected as experimental influencing factors. Measured intrinsic parameters—soil density, moisture content, Poisson's ratio, and shear modulus—were input into the EDEM database to obtain the range of values for soil JKR surface energy, collision recovery coefficient, and kinetic friction coefficient. Using the angle of repose (Y1) as the response variable and JKR, collision recovery coefficient, and kinetic friction coefficient as experimental factors, steepest slope climbing tests were conducted. The test plan and results are shown in Table 2.

Table 2

Steepest climbing test plan and results

Number	X_1 / (J·m^{-2})	X_2	X_3	Y_1 / (°)
1	0	0.15	0.15	39.06
2	0.6	0.27	0.13	41.55
3	1.2	0.39	0.11	44.60
4	1.8	0.51	0.09	48.81
5	2.4	0.63	0.07	50.93
6	3.0	0.75	0.05	55.43

As shown in Table 2, the third group of experiments yielded results closest to the true value. Using the third group as the central point, Box-Behnken experiments were conducted with the experimental factors in the second and fourth groups set at low and high levels, respectively. The experimental design and results are presented in Table 3, while the results of the analysis of variance are shown in Table 4.

Table 3

Box-Behnken experimental plan and results

Number	X_1/(N·m^{-3})	X_2	X_3	Y_1/(°)
1	0.6	0.39	0.13	42.87
2	1.2	0.27	0.09	45.73
3	1.2	0.39	0.11	45.8
4	1.8	0.39	0.13	46
5	1.2	0.51	0.09	49.73
6	0.6	0.27	0.11	43
7	1.8	0.39	0.09	49.97
8	0.6	0.51	0.11	43.25
9	1.2	0.39	0.11	45.96
10	1.2	0.39	0.11	44.1
11	0.6	0.39	0.09	42.35
12	1.2	0.27	0.13	44.67
13	1.2	0.51	0.13	49.08
14	1.2	0.39	0.11	45.54
15	1.8	0.51	0.11	49.25
16	1.8	0.27	0.11	45.3
17	1.2	0.39	0.11	45.04

Table 4

Stacking angle Box-Behnken experimental analysis of variance

Source	Sum of Squares	Degrees of Freedom	Mean Square	F	P
Model	89.81	9	9.98	12.49	0.0015**
X_1	45.36	1	45.36	56.76	0.0001**
X_2	19.88	1	19.88	24.87	0.0016**
X_3	3.33	1	3.33	4.16	0.0806
X_1X_2	3.42	1	3.42	4.28	0.0773
X_1X_3	5.04	1	5.04	6.31	0.0403*
X_2X_3	0.0420	1	0.0420	0.0526	0.8252
X_1^2	4.61	1	4.61	5.77	0.0473*
X_2^2	3.87	1	3.87	4.84	0.0637
X_3^2	4.70	1	4.70	5.88	0.0458*
Residual	5.59	7	0.7992		
Lack of fit	3.43	3	1.11	1.98	0.2590
Pure error	2.25	4	0.5625		
Sum	95.40	16			

*Note: * indicates significant difference (p<0.05), ** indicates extremely significant difference (P<0.01).*

Table 4 shows that the quadratic regression model for angle of repose Y_1 is highly significant, with the dissimilarity term being insignificant, indicating high model accuracy. The coded regression equations for angle of repose Y_1 are:

$$Y_1 = 45.29 + 2.38X_1 + 1.58X_2 - 0.645X_3 + 0.925X_1X_2 - 1.12X_1X_3 + 0.1025X_2X_3 - 1.05X_1^2 + 0.9585X_2^2 + 1.06X_3^2 \quad (11)$$

The optimum parameter set was identified as X_1 = 0.855 J/m², X_2 = 0.409, and X_3 = 0.126, achieving a Y_1 of 44. 42°. Substituting these optimized parameters into EDEM for simulation verification yielded simulated Y_1 values of 44.40°. The relative error compared to the true value was 0.05%.

The same calibration method was applied to calibrate the EDEM parameters for the 50–100 mm, 100–150 mm and 150–200 mm plough layer. The calibration results are shown in Table 5.

Table 5

EDEM parameters of plough layer soil at 50-100 mm, 100-150 mm, 150-200 mm

Plough layer/mm	X_1 / (J·m^{-2})	X_2	X_3	Y_1 / (°)	Error / %
50-100	2.102	0.626	0.125	45.84	0.22
100-150	2.180	0.681	0.124	47.83	0.15
150-200	2.221	0.621	0.15	49.76	0.08

Calibration of Residual Film Particle Contact Parameters

To enhance the precision of the residual film simulation model, this study introduced tensile distance as an additional response variable. Using Design-Expert software, a Box-Behnken design was created with tensile force Y_1 and tensile distance Y_2 as response variables. Normal stiffness, tangential stiffness, and bonding radius were set as experimental factors. High and low levels were defined as the upper and lower bounds of the values specified in Table 6, with three central points established. The experimental design and results are shown in Table 7, while the analysis of variance results are presented in Table 8.

Table 6

Factor level table for residual film tensile test

Factor	Parameter	Lower Level	Upper Level
X_1	Normal stiffness per unit area/(N·m^{-3})	5×10^7	9×10^7
X_2	Tangential stiffness per unit area/(N·m^{-3})	5×10^7	9×10^7
X_3	Bond radius/mm	0.23	0.25

Table 7

Box Behnken test plan and results

Number	X_1/(N·m^{-3})	X_2 / (N·m^{-3})	X_3 / mm	Y_1 / N	Y_2 / mm
1	9×10^7	5×10^7	0.24	1.823	13.6
2	9×10^7	7×10^7	0.25	1.889	17.6
3	5×10^7	5×10^7	0.24	1.804	10.4
4	7×10^7	9×10^7	0.23	1.879	9.6
5	9×10^7	7×10^7	0.23	1.848	18.4
6	7×10^7	9×10^7	0.25	1.926	11.2
7	7×10^7	5×10^7	0.25	1.831	17.6
8	5×10^7	7×10^7	0.23	1.828	15.2
9	5×10^7	9×10^7	0.24	1.894	12.8
10	7×10^7	5×10^7	0.23	1.799	12.0
11	9×10^7	9×10^7	0.24	1.919	13.6
12	5×10^7	7×10^7	0.25	1.910	10.4
13	7×10^7	7×10^7	0.24	1.855	27.2
14	7×10^7	7×10^7	0.24	1.850	26.4
15	7×10^7	7×10^7	0.24	1.845	26.4
16	7×10^7	7×10^7	0.24	1.793	24.0
17	7×10^7	7×10^7	0.24	1.811	24.0

Table 8

Analysis of variance in Box-Behnken experiment

Source	Y_1					Y_2				
	Sum of Squares	df	Mean Square	F	P	Sum of Squares	df	Mean Square	F	P
Model	0.0259	9	0.0029	5.78	0.0153*	575.60	9	63.96	8.91	0.0044**

Source	Y_1					Y_2				
	Sum of Squares	df	Mean Square	F	P	Sum of Squares	df	Mean Square	F	P
X_1	0.0002	1	0.0002	0.4640	0.5177	25.92	1	25.92	3.61	0.0991
X_2	0.0163	1	0.0163	32.70	0.0007**	5.12	1	5.12	0.7134	0.4262
X_3	0.0051	1	0.0051	10.24	0.0151*	0.32	1	0.32	0.0446	0.8388
X_1X_2	9×10^{-6}	1	9×10^{-6}	0.0181	0.8969	1.44	1	1.44	0.2006	0.6677
X_1X_3	0.0004	1	0.0004	0.8436	0.3889	4.00	1	4.00	0.5573	0.4797
X_2X_3	0.0001	1	0.0001	0.1129	0.7467	4.00	1	4.00	0.5573	0.4797
X_1^2	0.0016	1	0.0016	3.25	0.1146	109.52	1	109.52	15.26	0.0059**
X_2^2	0.0004	1	0.0004	0.7790	0.4067	262.78	1	262.78	36.61	0.0006**
X_3^2	0.0014	1	0.0014	2.85	0.1355	109.52	1	109.52	15.26	0.0059**
Residual	0.0035	7	0.0005			50.24	7	7.37		
Missing term	0.0005	3	0.0002	0.2285	0.8724	41.28	3	13.76	6.14	0.0560
Pure error	0.0030	4	0.0007			8.96	4	2.24		
Sum	0.0294	16				625.84	16			

*Note: * indicates significant difference (p<0.05), ** indicates extremely significant difference (P<0.01).*

Table 8 shows that both the tensile force Y_1 and tensile distance Y_2 exhibit highly significant quadratic regression models, with insignificant error terms, indicating high model accuracy. In the linear terms of this model, X_2 is highly significant for tensile force Y_1 (P<0.01), X3 is significant for Y_1 (P<0.05), while X_1 is not significant for Y_1 (P>0.05). The encoded regression equations for tensile force Y_1 and tensile distance Y_2 are respectively:

$$Y_1=1.83+0.0054X_1+0.0451X_2+0.0252X_3+0.0015X_1X_2-0.0102X_1X_3 +0.0038X_2X_3+0.0196X_1^2+0.0196X_2^2+0.0184X_3^2 \quad (12)$$

$$Y_2=25.6+1.8X_1-0.8X_2+0.2X_3-0.6X_1X_2+X_1X_3-X_2X_3-5.1X_1^2-7.9X_2^2-5.1X_3^2 \quad (13)$$

Using Design-Expert software for optimization, the parameters X1, X2, and X3 were determined to be 7.49×10^7 N·m^{-3}, 7.52×10^7 N·m^{-3}, and 0.243 mm, respectively, while Y1 and Y2 were found to be 1.877 N and 25.158 mm, respectively. The optimized parameter combinations were validated through simulation experiments in EDEM, yielding simulated values of Y1=1.874 N and Y2=25.6 mm. The relative errors compared to actual values were 0.160% and 0.934%, respectively. The relationships between tensile displacement and tensile force in the actual and simulated tensile test are shown in Figure 6.

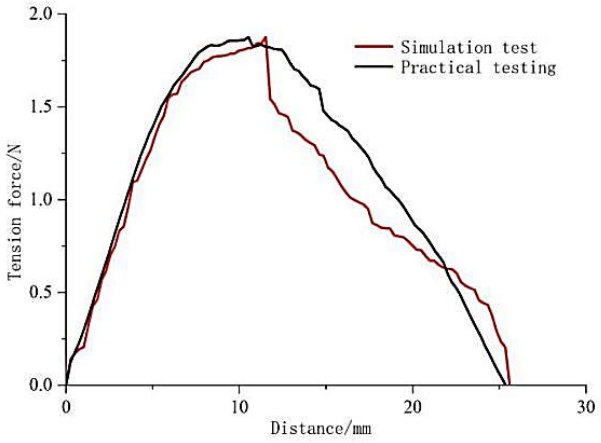

Fig. 6 - Average tensile property values between simulation and actual tests of residual Film

Validation of the coupled EDEM model

The coupled EDEM model of soil-residual film was established via modular modelling and hierarchical calibration. Based on the statistical size characteristics and spatial distribution of residual film in the target area,

an appropriate number of residual film sub-models and soil sub-models were randomly and alternately generated. Using the established soil-residual film coupled EDEM model, a simulation of the angle of repose was conducted. As shown in Figure 7, the simulated angle of repose was 50.90°, while the physical test yielded 50.38°, resulting in an error of 1.03%. The comparison indicates no significant difference between the simulation and experimental results.

（a）Simulation test （b）Physical test

Fig. 7 - Comparison of simulation and physical tests

CONCLUSIONS

(1) For soils at different plough layer depth, a soil simulation model was established using the Hertz-Mindlin with JKR model. Using angle of repose as the experimental metric, the JKR surface energy, collision recovery coefficient, static friction coefficient, and dynamic friction coefficient between soil particles were systematically calibrated through steepest ascent tests and Box-Behnken experiments.

(2) A residual film simulation model was constructed using the Hertz-Mindlin with Bonding model in EDEM. The parameters for the Bonding model were calibrated based on tensile tests, and model parameters were optimized using Box-Behnken experiments. Simulated tensile test using the optimized parameters yielded simulated tensile force and distance values of 1.87 N and 25.6 mm, respectively, with relative errors of 0.160% and 0.934% compared to actual measurements.

(3) Employing a block-based modelling approach, layered soil and residual film models of different sizes (<4 cm², 4–25 cm², >25 cm²) were integrated to construct a high-precision coupled discrete element simulation model of layered soil-residual film. The model was validated through a repose angle simulation, yielding a result of 50.90°, which showed a 1.03% error compared to the physical test result of 50.38%, indicating no significant difference.

ACKNOWLEDGEMENT

This work was supported by National Natural Science Foundation of China (32472013); Xinjiang Uygur Autonomous Region “Challenge-Based Project” on the Development and Application of High-Quality and Efficient Mechanical Recycling Technology and Equipment for Agricultural Film Residues in Farmland; Jiangsu Province University Natural Science Research Key Project (19KJA430018).

REFERENCES

[1] Al-Hashemi HMB., Al-Amoudi, (2018). A review on the angle of repose of granular materials. *Powder Technology*, vol.330, pp.397-417. DOI:10.1016/j.powtec.2018.02.003

[2] Chen F., Yang L., Cui T., Zhang D., He X., Zhang K. (2025). Establishment and parameter calibration of the discrete element model for typical clay in hilly and mountainous areas. *International Journal of Agricultural and Biological Engineering*, vol.18, pp.26-38. DOI:10.25165/j.ijabe.20251805.9794

[3] Chen J., Krengel D., Nishiura D., Furuichi M., Matuttis H.G., (2023). A force-displacement relation based on the JKR theory for DEM simulations of adhesive particles. *Powder Technology*, vol.427, pp.1-17. DOI:10.1016/j.powtec.2023.118742

[4] Fang W., Wang X., Han D., Zang N., Chen X., Ohiemi I., (2024). Parameter optimization and disturbance analysis of the film picking device of the chain-type plough layer residual film recovery machine based on DEM-MBD coupling. *Computers and Electronics in Agriculture*, vol.222, pp.1-15. DOI:10.1016/j.compag.2024.109041

[5] Fang W., Wang X., Han D., Ohiemi I., (2025). Design and Testing of Film Picking-Unloading Device of Tillage Residual Film Recycling Machine Based on DEM Parameter Calibration. *Agronomy-Basel*, vol.15, pp.1-20. DOI:10.3390/agronomy15040955

[6] Feng Y., Owen D., (2014). Discrete element modelling of large scale particle systems—I: exact scaling laws. *Computational Particle Mechanics*, vol.1, pp.159-168. DOI:10.1007/s40571-014-0010-y

[7] He R., Duan Q., Chen X., Xu G., Ding Q., (2022). DEM Analysis of Spatial Distribution Quality of Rotary Tillage Straw Returning (旋耕还田秸秆空间分布质量离散元分析). *Transactions of the Chinese Society for Agricultural Machinery*, vol.53, pp.44-53. DOI: 10.6041/j.issn.1000-1298.2022.06.004

[8] Hu C., Wang X., Chen X., Tang X., Zhao Y., Yan C., (2019). Current situation and control strategies of residual film pollution in Xinjiang (新疆农田残膜污染现状及防控策略). *Transactions of the Chinese Society of Agricultural Engineering*, vol.35, pp.223-234. DOI: 10.11975/j.issn.1002-6819.2019.24.027

[9] Hu Q., Li X., Shi H., Chen N., Zhang Y., Ma H., (2021). Response of maize root to residual plastic film and root distribution model in Hetao Irrigation District of Inner Mongolia (河套灌区玉米根系对残膜的响应及根系分布模型). *Transactions of the Chinese Society of Agricultural Engineering*, vol.37, pp.143-152. DOI: 10.11975/j.issn.1002-6819.2021.21.017

[10] Huang C., Jian L., Chen X., Wang F,. An P., (2018). Research on the effects of plastic film mulching and seedling transplanting on crop yield and water and heat resource utilization (地膜覆盖和育苗移栽技术对农作物产量和水热资源利用的影响). *Journal of China Agricultural University*, vol.23, pp.1-12. DOI:10.11841/j.issn.1007-4333.2018.12.01

[11] Jin W., Ding Y., Nong F., Zhang X., Bai S., (2023). Design and Test of Excavating and Conveying Device with Vibrating Chain Tooth and Bar for Residual Film-Soil-Straw (抖动链齿杆式残膜-土壤-秸秆挖掘与输送装置设计与试验). *Transactions of the Chinese Society for Agricultural Machinery*, vol. 54, pp.71-82. DOI: 10.6041/j.issn.1000-1298.2023.11.007

[12] Li H., Li S., Nan L., Li H., Guo Q., (2017). Meta-analysis of Effect of Plastic Film Mulching Cotton Yield in China (中国棉花地膜覆盖产量效应的 Meta 分析). *Transactions of the Chinese Society for Agricultural Machinery*, vol.48, pp.228-235. DOI: 10.6041/j.issn.1000-1298.2017.07.029

[13] Li, S., Diao P., Miao H., Zhao Y., Li X., Zhao H., (2024). Modeling the fracture process of wheat straw using a discrete element approach. *Powder Technology*, vol. 439, pp.1-11. DOI: 10.1016/j.powtec.2024.119762

[14] Li S., Huan X., Wang T., Hui Y., You Y., Wang D., (2024). Biomechanical properties and discrete element modeling of PSR stalks during silage harvest. *Computers and Electronics in Agriculture*, vol.217, pp.1-16. DOI: 10.1016/j.compag.2024.108644

[15] Liang R., Chen X., Zhang B., Meng H., Jiang P., Peng X., Kan Z., Li W., (2019). Problems and countermeasures of recycling methods and resource reuse of residual film in cotton fields of Xinjiang (新疆棉田残膜回收方式及资源化再利用现状问题与对策). *Transactions of the Chinese Society of Agricultural Engineering*, vol.351, pp.13. DOI: 10.11975/j.issn.1002-6819.2019.16.001

[16] Liu F Y, Zhang J, Li B, Chen J., (2016), Calibration of parameters of wheat required in discrete element method simulation based on repose angle of particle heap (基于堆积试验的小麦离散元参数分析及标定). *Transactions of the Chinese Society of Agricultural Engineering*, 32(12): 247-253. DOI: 10.11975/j.issn.1002-6819.2016.12.035

[17] Li Y., Li F., Xu X., Shen C., Meng K., Chen J., Chang D., (2019). Parameter calibration of wheat flour for discrete element method simulation based on particle scaling (基于颗粒缩放的小麦粉离散元参数标定). *Transactions of the Chinese Society of Agricultural Engineering*, vol.35, pp.320-327. DOI: 10.11975/j.issn.1002-6819.2019.16.035

[18] Queteschiner D., Lichtenegger T., Pirker S., Schneiderbauer S., (2018). Multi-level coarse-grain model of the DEM. *Powder Technology*, vol.338, pp.614-624. DOI: 10.1016/j.powtec.2018.07.033

[19] Ren J., Zhou L., Han L., Zhou J., Yan M., (2017). Discrete Simulation of Vertical Screw Conveyor Based on Particle Scaling Theory (基于颗粒缩放理论的垂直螺旋输送离散模拟). *The Chinese Journal of Process Engineering*, Vol.17, pp.936-943. DOI: 10.12034/j.issn.1009-606X.217109

[20] Shen S., Zhang J., Jiang Y., Wang Y., Liu X., Li, Dong W., (2024). Tensile Properties of Residual Film in Tillage Layer Based on Discrete Element Method (基于离散元法的耕层残膜拉伸性能研究). *Transactions of the Chinese Society for Agricultural Machinery*, vol.55, pp.132-141. DOI: 10.6041/j.issn.1000-1298.2024.07.013

[21] Song S., Tang Z., Zheng X., Liu J., Meng X., Liang Y., (2021). Calibration of the discrete element parameters for the soil model of cotton field after plowing in Xinjiang of China (新疆棉田耕后土壤模型离散元参数标定). *Transactions of the Chinese Society of Agricultural Engineering*, vol. 37, pp.63-70. DOI: 10.11975/j.issn.1002-6819.2021.20.007

[22] Thakur S., Ooi J., Ahmadian H., (2016). Scaling of discrete element model parameters for cohesionless and cohesive solid. *Powder Technology*, vol.293, pp.130-137. DOI: 10.1016/j.powtec.2015.05.051

[23] Wang X., Chen X., Sun D., Kang J., Peng Q., Zhang C., (2025). Research progress and prospects of technology and equipment for controlling residual film pollution in farmland (农田残膜污染治理技术及装备研究进展与展望). *Agricultural Equipment & Vehicle Engineering*, vol.63, pp.1-9. DOI: 10.3969/j.issn.1673-3142.2025.01.001

[24] Yang L., Heng T., He X., Yang G., Li Y., Xu Y., (2023). Spatial-temporal distribution and accumulation characteristics of residual plastic film in cotton fields in arid oasis area and the effects on soil salt transport and crop growth. *Soil & Tillage Research*, vol.231, pp. 1-15. DOI: 10.1016/j.still.2023.105737

[25] Yu Z., Xiong W., Zhu D., Xue K., Zhang S., Kuang F., Que J., Zhang X., Heng B., (2022). Analysis and calibration of parameters of wet-viscous paddy mud particles based on the slump experiment. *INMATEH-Agricultural Engineering*, vol.68, pp.177-190. DOI: 10.35633/inmateh-68-18

[26] Zhang B., Yang X., Wang J., Chen J., Shen W., (2024). Construction of a rheological model based on discrete element parameters calibration of clay from sugarcane cultivated land (基于甘蔗耕地黏土离散元参数标定的流变模型构建). *Transactions of the Chinese Society of Agricultural Engineerin*g, vol.40, pp.36-44. DOI: 10.11975/j.issn.1002-68 19.202311137

[27] Zhang X., Yu S., Hu X., Zhang L., (2024). Study on rotary tillage cutting simulations and energy consumption predictions of sandy ground soil in a Xinjiang cotton field. *Computers and Electronics in Agriculture*, vol.217, pp.1-12. DOI: 10.1016/j.compag.2024.108646